Translational Oncology
www.transonc.com

Volume 10 Number xx Month 2017 pp. 311–317 311

# Early Lung Adenocarcinoma in Mice: Micro-Computed Tomography Manifestations and Correlation with Pathology[1]

**Lin Deng[2], Shi Man Xiao[2], Jin Wei Qiang, Yong Ai Li and Yu Zhang**

Department of Radiology, Jinshan Hospital & Shanghai Medical College, Fudan University, Shanghai, 201508, China

## Abstract

Lung cancer is the most common fatal malignancy for both men and women and adenocarcinoma is the most common histologic type. Early diagnosis of lung cancer can significantly improve the survival rate of patients. This study aimed to investigate the micro-computed tomography (micro-CT) manifestations of early lung adenocarcinoma (LAC) in mice and to provide a new perspective for early clinical diagnosis. Early LAC models in 10 mice were established by subcutaneously injecting 1-methyl-3-nitro-1-nitrosoguanidine (MNNG) solution. Micro-CT scan and multiple planar reconstruction (MPR) were used for mouse lungs. Micro-CT features of early LAC, especially the relationships between tumor and bronchus, were analyzed and correlated with pathology. Micro-CT findings of early LAC were divided into three types: non-solid (n = 8, 6%), partly solid (n = 85, 64%) and totally solid (n = 39, 30%). Tumor-bronchus relationships, which could be observed in 110 of 132(83%) LAC, were classified into four patterns: type I (n = 16, 15%), bronchus was truncated at the margin of the tumor; type II (n = 33, 30%), bronchus penetrated into the tumor with tapered narrowing and interruption; type III (n = 38, 35%), bronchus penetrated into the tumor with a patent and intact lumen; type IV (n = 99, 90%), bronchus ran at the border of the tumor with an intact or compressed lumen. Micro-CT manifestations of early LAC correlated well with pathological findings. Micro-CT can clearly demonstrate the features of mouse early LAC and bronchus-tumor relationships, and can also provide a new tool and perspective for the study of early LAC.

*Translational Oncology (2017) 10, 311–317*

## Introduction

Lung cancer remains the leading incidence of malignant tumor, accounting for male and female cancer mortality rates of 28% and 26%, respectively [1,2]. CT screening for lung cancer has been shown to obviously reduce lung cancer mortality in a series of recent randomized controlled trials [3–7]. Consequently, low-dose computed tomography (CT) has been widely used for lung cancer screening and has detected a large number of small or micro lung nodules that pose a diagnostic challenge to radiologists. Among the lung nodules found by screening CT in a high risk population, 1.1% to 12% of them were malignant and most of them were lung adenocarcinomas (LAC) [8–11]. However, these early LAC lack characteristic CT findings, such as lobulation, speculation and contrast-enhancement. Therefore, it is difficult to make a correct diagnosis for early LAC [12,13]. Furthermore, most of the tumors were too small to obtain a complete tissue sample after the intraoperative frozen section diagnosis, which led to a restricted CT-pathology correlation. Micro-computed tomography (micro-CT) of lung cancer in animal models can make up for the limitations of clinical study. In contrast to clinical CT, micro-CT possesses micron-sized resolution, which can show anatomical micro-structure information [14,15]. Enabled by the inherent contrast between air and tissue, micro-CT is a powerful modality for lung imaging and can clearly show the characteristics of

Address all correspondence to: Jin Wei Qiang, Department of Radiology, Jinshan Hospital & Shanghai Medical College, Fudan University, Shanghai, 201508, China.
E-mail: dr.jinweiqiang@163.com.

[1] This work was supported by National Natural Science Foundation of China [81171340]; and The Science and Technology Commission of Shanghai, Shanghai [10411956800].

[2] Lin Deng and Shi Man Xiao contributed equally to this work and were co-first authors.

Received 13 January 2017; Revised 16 February 2017; Accepted 16 February 2017



1936-5233/17
http://dx.doi.org/10.1016/j.tranon.2017.02.003

early mouse LAC and also provide a novel viewpoint and tool for the study of LAC.

Based on the pre-established mouse model of early LAC [16], this study aimed to investigate micro-CT manifestations of early LAC and tumor-bronchus relationship to afford new information for clinical CT diagnosis.

## Materials and Methods

### *Establishment of Mouse Model and Animal Preparation*

The study was approved by the institutional review board of Jinshan Hospital, Fudan University. Every effort was made to minimize suffering and the number of animals used in each experiment.

As previously described [16], early LAC models were established in 10 female KM mice (Jie Si Jie Laboratory Animal Company, Shanghai, China) by subcutaneously injecting 0.2 ml 1-methyl-3-nitro-1-nitrosoguanidine (MNNG) solution (2.0 mg/ml) (Ru Ji Biotech Company, Shanghai, China) once weekly for 4 weeks. At the 100th day after the first injection, animals were anesthetized by intraperitoneal injection of 0.02 ml ketamine solution (10 mg/ml). The trachea was exposed via a midline neck incision. A 50% dose of silica solution 0.4 ml was administered through the inferior vena cava to induce pulmonary embolism and consequent deep breathing. The trachea was ligated rapidly at the end of deep inspiration to maintain lung inflation. The mice were euthanized by cervical dislocation and immersed in 10% formalin solution for 24 h.

### *Micro-CT Scanning and Imaging Analysis*

Mice chests were scanned by micro-CT equipment (Siemens in vivo micro-CT) with a field of view 24 mm × 24 mm. According to the pre-experimental results, acquisition parameters were chosen as follows: data acquisition method bin1, resolution 19.0 μm, voltage 80 kV, current 500 μA, time exposure 600*3 ms, scanning time 64 min and magnification 5.0. Multiple planar reconstruction (MPR) of lung images in three orthogonal planes was performed with the reconstruction algorithm dsf2 and matrix size 2048*2048 by using a post-processing workstation (Inveon research worksystem). Three lung lobes of each mouse were randomly selected and the number, diameter, margin and solid component of tumors were analyzed and recorded in transverse, sagittal and coronal reconstructed images. The interior or exterior bronchi of tumor and the tumor-bronchus relationships were observed emphatically. The spatial relationships between bronchus and tumor were defined according to the following methods: (1) central bronchus: bronchus located within the area of central 1/2 radius of tumor; (2) peripheral bronchus: bronchus located in the area of peripheral 1/2 radius of tumor; (3) exterior bronchus: bronchus bordered tumor. The sequential imaging sections that were identical with the pathological sections were reconstructed in 37 focused tumors, by referring the tumor's pathological shape and its adjacent large vessels and pleura.

### *Histopathologic Analysis*

The lung lobe of each mouse was separated, grossly observed for nodules, and fixed in neutral formalin. The 3-mm-block included a nodule that was sampled and embedded in paraffin. The whole paraffin block was cut into a series of 3-μm sections, with an interval of 100 μm. Sections were stained with hematoxylin and eosin (H&E) and were microscopically analyzed to determine the histologic type, in addition to the size, shape, margin, growth pattern and bronchus of the tumor. Thirty-seven tumors were selected to strictly correlate between the micro-CT findings and pathology, focusing on the tumor-bronchus relationship.

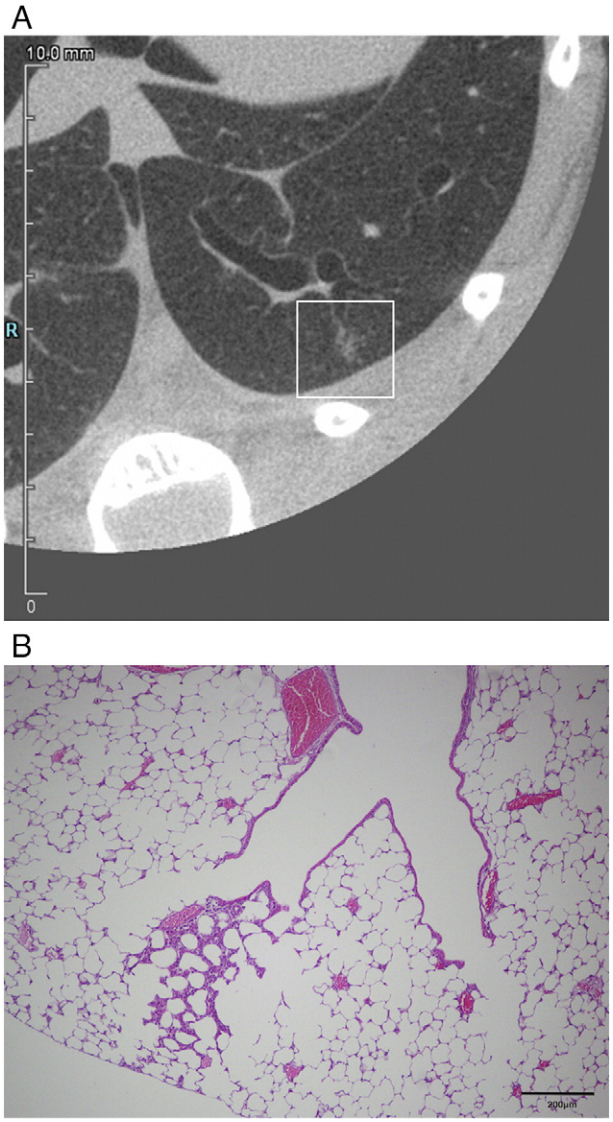


**Figure 1.** Micro-CT and photomicrograph (HE ×100) of a non-solid tumor. Micro-CT (A) shows an irregular non-solid nodule (white box), which appears as ground-glass opacity with cribriform lucent structures and proximal bronchioli. Photomicrograph (B) shows that the tumor cells grow along the alveolar septa, and intact alveoli and patent border bronchioli with an intact mucosa.

### *Statistical Analysis*

Statistical analyses were performed using SPSS 20.0 statistical software (SPSS Inc., Chicago, IL, USA). A Pearson chi-square test was conducted to compare the relationships both between tumor size and bronchial position in groups of partly solid and totally solid tumors, and between tumor size and tumor-bronchus relationship patterns. A *P*-value of less than .05 was considered to be a statistically significant difference.

## Results

### *Micro-CT Manifestations of Tumors*

All 10 mice had tumor formation. The number of tumors ranged from 9 to 47, with a total of 231 tumors found by micro-CT. Three lobes were randomly selected from each mouse, and a total of 132 tumors were investigated. All the tumors were LAC that were confirmed by histology. The tumor size ranged from 0.1 mm to 1.8 mm, with a mean diameter of 0.56 mm.

Micro-CT findings of LAC were classified into three types based on the proportion of the solid component: non-solid (n = 8, 6%), partly solid (n = 85, 64%) and totally solid (n = 39, 30%). A non-solid tumor appeared as a well-defined, irregular ground-glass opacity with cribriform or tube-like lucent structures and spicular margin (Figure 1). A partly solid tumor appeared as a well-defined, irregular nodule with a central solid, peripheral ground-glass opacity and spicular margin. There were cribriform or tube-like low density structures in the peripheral ground-glass opacity (Figure 2). A totally solid tumor was a homogeneous solid density nodule with a smooth margin (Figure 3).

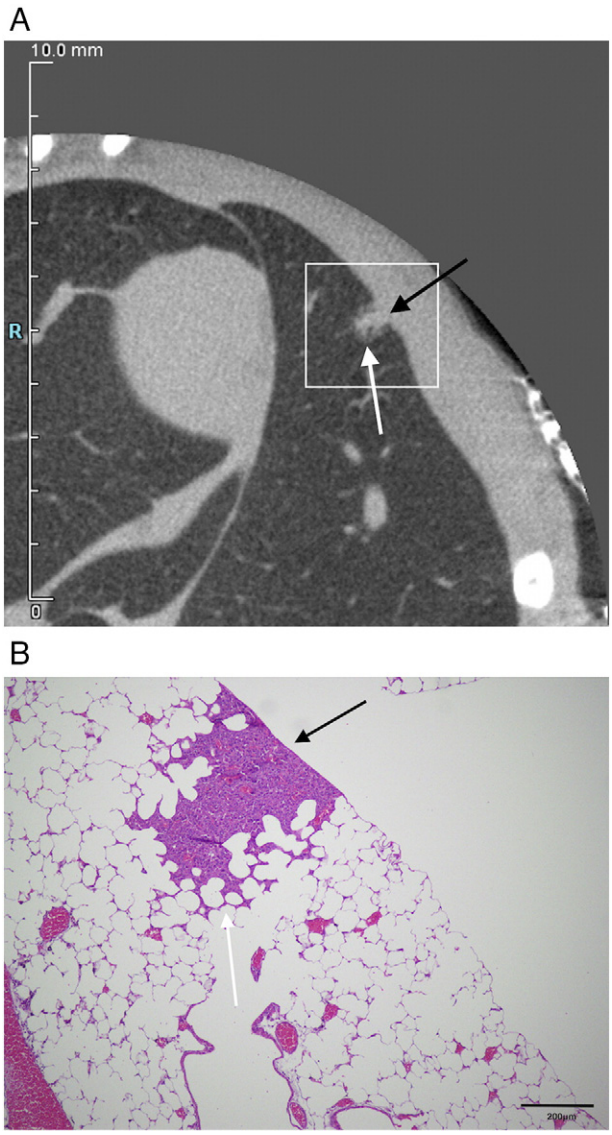


**Figure 2.** Micro-CT and photomicrograph (HE ×100) of a partly solid tumor. Micro-CT (A) shows that a partly solid nodule (white box) appears as a central solid with a homogeneous high density (black arrow); peripheral ground-glass opacity (white arrow) with cribriform and tube-like structures. Photomicrograph (B) shows a mixed growth pattern tumor. The center and periphery of the tumor appear as hilic (black arrow) and lepidic (white arrow) growth, respectively. There are intact alveoli and alveolar ducts in the periphery of the tumor that correlate with the cribriform or tube-like structures on micro-CT.

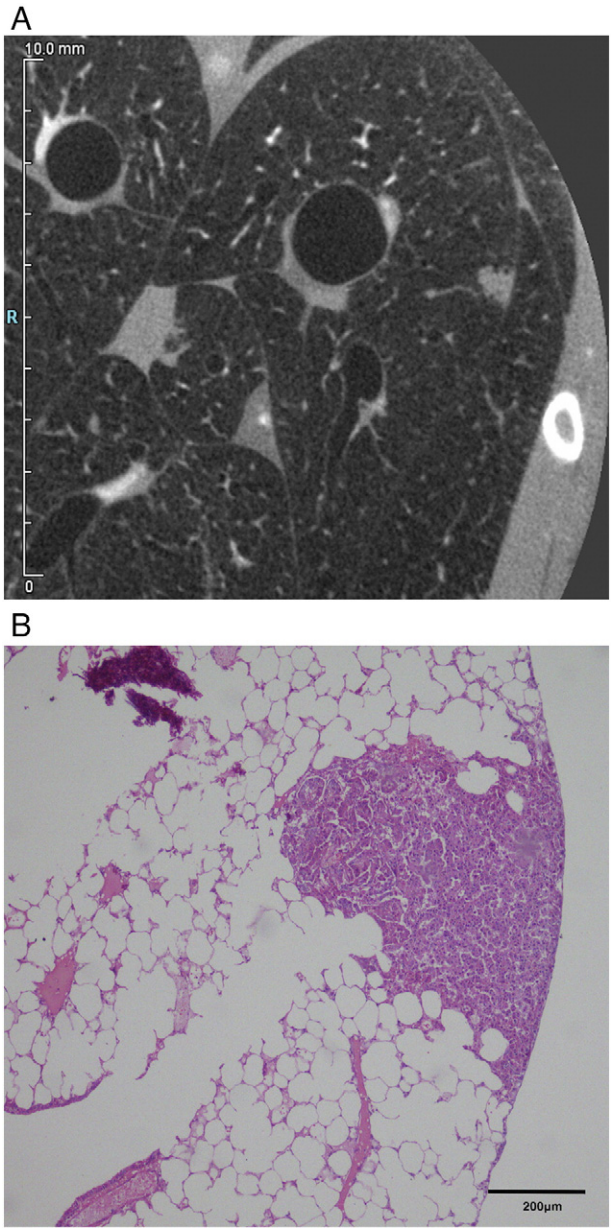


**Figure 3.** Micro-CT and photomicrograph (HE ×100) of a totally solid tumor. Micro-CT (A) shows a homogeneous solid nodule with a high density, smooth margin and some little round lucent structures (white box). Photomicrograph (B) shows a hilic growth tumor without intratumoural air-contained alveoli and patent bronchioli. There are some air-contained alveoli and patent bronchioli in the border of the tumor that correlate with little round lucent structures on micro-CT.

### *Tumor-Bronchus Relationship*

One hundred ten (83%) out of 132 tumors had a direct relation with bronchus. The tumor-bronchus relationships were classified into four types as follows: type I (n = 16, 15%), bronchus was truncated at the margin of the tumor (Figure 4); type II (n = 33, 30%), bronchus penetrated into the tumor with tapered narrowing and interruption (Figure 5); type III (n = 38, 35%), bronchus penetrated into the tumor with a patent and intact lumen (Figure 6); and type IV (n = 99, 90%), bronchus ran at the border of the tumor with an intact or compressed lumen (Figure 7). With increased tumor size, the prevalence of type I tumor-bronchus relationship increased, whereas types II and III decreased, and type IV was mostly observed in medium-sized tumors. There were significant differences in the prevalence of tumor-bronchus patterns among different tumor sizes ($P$ = .006). The relationship between tumor size and tumor-bronchus pattern is listed in Table 1.

Non-solid tumors were frequently less than 0.5 mm in diameter. The bronchus appeared as little round or tube-like lucent structures that penetrated into the center and the periphery of the tumor. The bronchus in partly solid and totally solid tumors were located at the center, periphery and exterior border of the tumor with an increasing prevalence. The bronchus could be found at the exterior border in almost all of partly solid tumors, whereas the prevalence of this occurrence was relatively less in totally solid tumors. The distributions of bronchus in partly solid and totally solid tumors are listed in

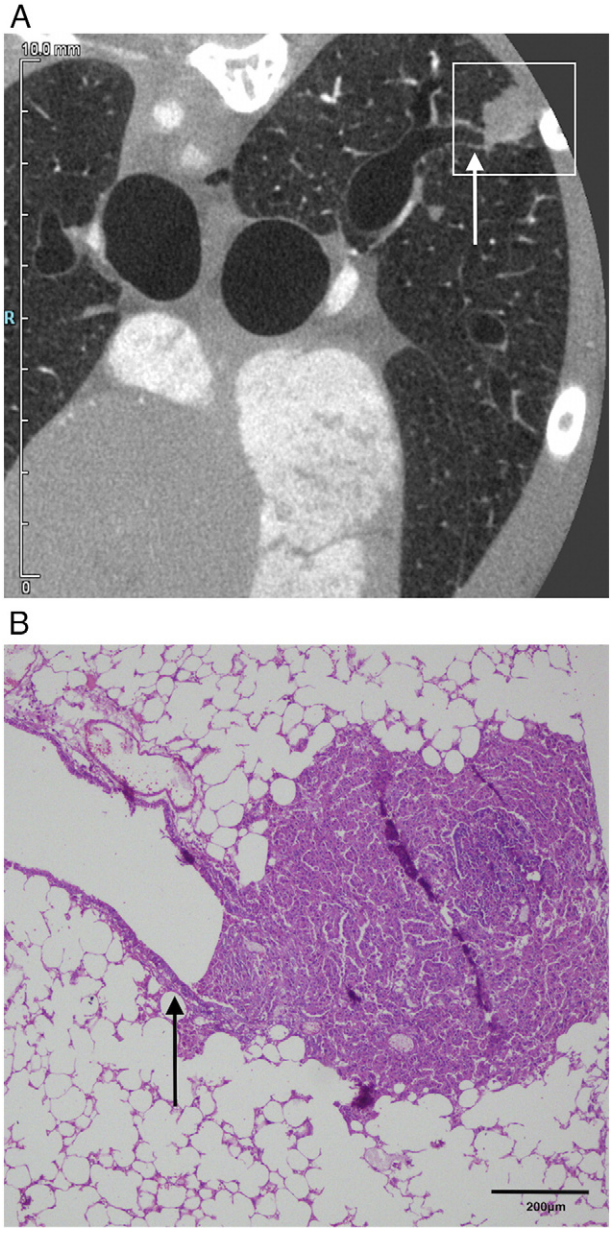


**Figure 4.** Type I tumor–bronchus relationship. Micro-CT (A) shows that a bronchus (white arrow) is obstructed abruptly by a totally solid tumor (white box). The slightly thickened-wall is seen in the bordering portion of the bronchus (white arrow). (B) Photomicrograph (HE ×100) of the same tumor shows an identical tumor–bronchus relationship with a slightly thickened-wall of the bronchus both inside and outside the tumor (black arrow).

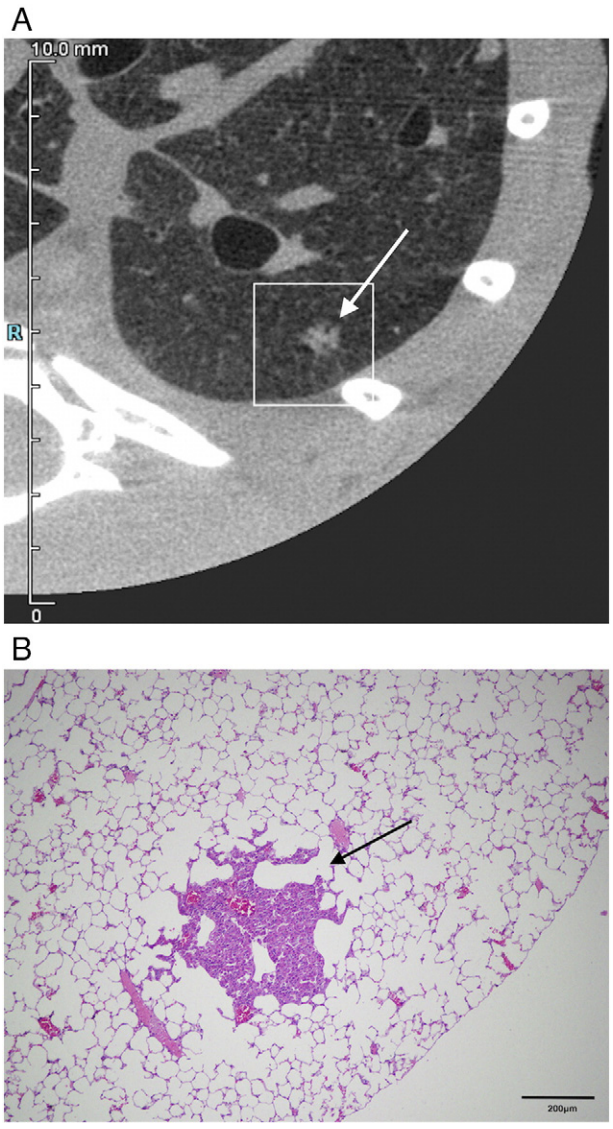


**Figure 5.** Type II tumor–bronchus relationship. Micro-CT (A) shows that a bronchioli (white arrow) penetrates into an irregular partly solid tumor (white box) and interruption. Photomicrograph (HE ×100) of the same tumor (B) shows an identical tumor–bronchus relationship. The bronchioli (black arrow) and intratumoural alveolar ducts correlate with the tube-like and round lucent structures on micro-CT.

Table 2. There were significantly statistical differences in the prevalence of bronchus among different locations of partly solid and totally solid tumors ($P < .001$, $P = .003$).

### *Histopathological Findings*

Histopathologically, the tumors demonstrated three types of growth patterns: lepidic, hilic and mixed, which corresponded to non-solid, totally solid and partly solid tumors on micro-CT. No tumor cells were found in all ventilating bronchioles. Varying envelop, compression and invasion were found in respiratory bronchioles. Tumor cells proliferated, accumulated and extended inside the alveolar septa, and compressed, diminished and obliterated the alveoli to varying degrees. The lepidic tumor evolved into the mixed and hilic tumors. On micro-CT, the heterogeneous ground-glass opacity and cribriform structures corresponded pathologically to the thickened neoplastic alveolar septa and alveoli, respectively; the little round or tube-like lucent structures inside the tumor were the residual alveoli, alveolar ducts or patent bronchioli. The lepidic tumor cells were either hindered by the bronchioli and bronchus or grew around them, or both, in the process of spreading along the alveolar septa, and thus formed a well-defined margin

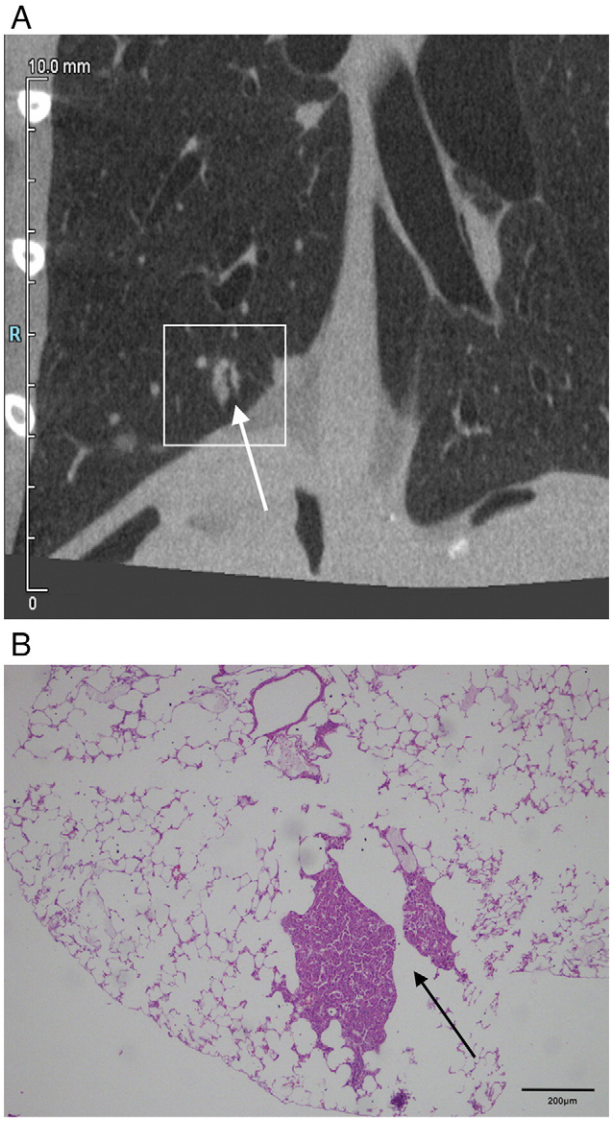


**Figure 6.** Type III tumor–bronchus relationship. Micro-CT (A) shows a bronchiole (white arrow) run through a solid tumor (white box) with a patent and intact lumen. Photomicrograph (HE ×100) of the same tumor (B) show a corresponding bronchiole (black arrow) with a smooth lumen.

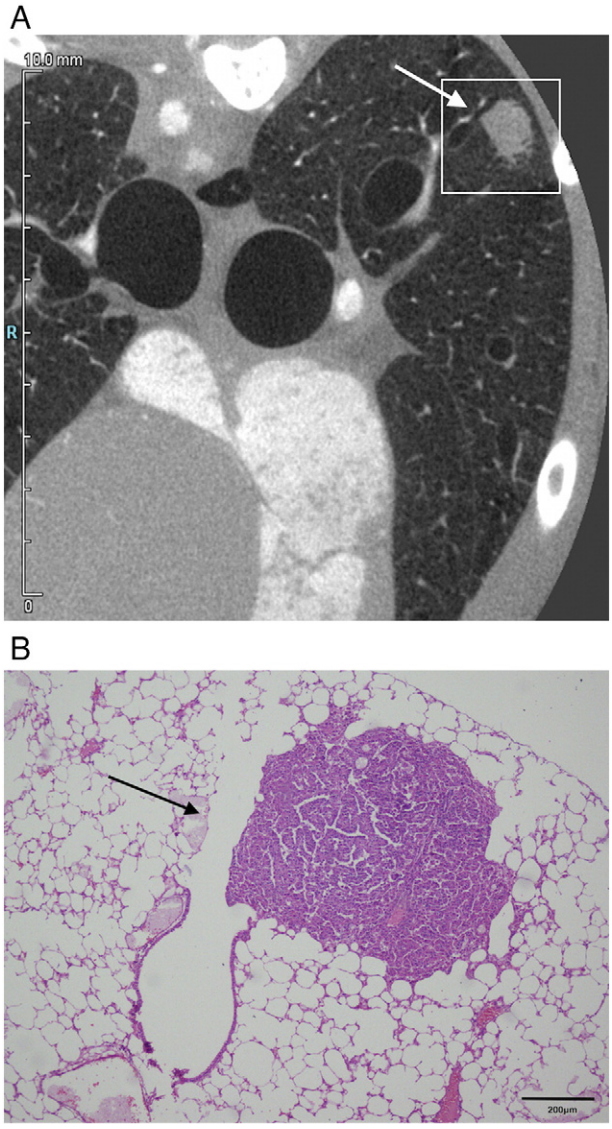


**Figure 7.** Type IV tumor–bronchus relationship. Micro-CT (A) shows a bronchiole (white arrow) runs at the border of a solid tumor (white box) with an intact lumen. Photomicrograph (HE ×100) of the same tumor (B) shows a corresponding bronchiole (black arrow) at the border of the tumor.

**Table 1.** The Correlation Between Tumor Size and Tumor-Bronchus Relationship

| Tumor–Bronchus Relationships | Total | Tumor Size (n = 110) | | | *P*-Value* |
|---|---|---|---|---|---|
| | | 0–0.5 (45) | 0.5–1.0 (60) | 1.0–2.0 (5) | |
| Type I | 16 (15%) | 4 (9%) | 10 (17%) | 2 (40%) | .008 |
| Type II | 33 (30%) | 19 (42%) | 13 (22%) | 1 (20%) | .000 |
| Type III | 38 (35%) | 27 (60%) | 11 (18%) | 0 (0%) | .000 |
| Type IV | 99 (90%) | 41 (68%) | 54 (90%) | 4 (80%) | .000 |
| *P*-value* | .000 | .000 | .000 | .083 | / |

* Pearson $\chi 2$ test.

**Table 2.** The Distributions of Bronchi in Partly Solid and Totally Solid Tumors

| Tumor Number | Bronchial Location | | | *P*-Value* |
|---|---|---|---|---|
| | Centre | Periphery | Exterior | |
| Partly solid (n = 85) | 18 (21%) | 41 (48%) | 80 (94%) | .000 |
| Totally solid (n = 39) | 6 (15%) | 16 (41%) | 20 (51%) | .003 |

* Pearson $\chi^2$ test.

(bronchus parallel to image section) and a lobulation (bronchus perpendicular to image section), or an irregular shape, or spiculation. Micro-CT manifestations were precisely correlated with pathological findings in 37 focused tumors; type I tumor-bronchus relationship was seen in 8 (22%) tumors, type II was seen in 13 (35%) tumors, type III was seen in 14 (38%) tumors, and type IV was seen in 33 (89%) tumors.

## Discussion

### *The Advantages of Micro-CT in Investigating Mouse Lung Cancer Model*

In the present study, micro-CT, with a resolution of 19 μm, was used to investigate early LAC in mice. The results indicated that micro-CT could clearly demonstrate the morphological characteristics of the tumor and tumor-bronchus relationship. Previous studies [17–23] used micro-CT to investigate the vessel supply, angiogenesis and therapeutic response of mouse lung cancer, as well as airway changes in a mouse asthma model. However, it could only demonstrate the presence of lung tumors and could not clearly show the internal structure of tumors. Because of the motion artifacts caused by the respiration or cardiac impulse of mice, it was difficult to obtain clear images in vivo [23]. Furthermore, the spatial resolution in previous studies was not high enough to obtain a satisfactory image. In this study, a state-of-the-art micro-CT scanner, with a 19-μm high resolution, and sacrificed mice were used to conduct a lung scan. In this way, the airways, from the biggest trachea to the smallest alveolar tube, were clearly displayed, and tumor-bronchus relationships could be thoroughly investigated.

Since the resolution of micro-CT is far superior to that of clinical CT, it can provide more information about small bronchi, bronchioli and tumor-bronchus relationships [24]. Our study showed that micro-CT display multiple tumor relevant bronchi in 78% of tumors and multiple types of tumor-bronchus relationship in 64% of tumors. The results suggested that the tumor-bronchus relationship was a prevalent CT sign, which was applied to investigate the occurrence and progression of tumors.

### *The Correlation Between Micro-CT Findings and Pathological Growth Patterns of Tumors*

Our study showed that micro-CT findings of mouse LAC could be divided into three categories: non-solid, partly solid, and totally solid nodules that pathologically corresponded to three growth patterns: lepidic, mixed and hilic. Meanwhile, these three categories of micro-CT findings corresponded to pure ground-glass, mixed ground-glass and solid nodules on clinical CT [25,26]. Owing to its micron-size resolution capability, micro-CT identify the compressed and residual alveoli, alveolar ducts and bronchioli, which appeared as cribriform or tube-like lucent structures delineated by the thickened neoplastic alveolar septa in non-solid nodules and the periphery of partly solid nodules. It is well known that LAC cells originate from alveolar epithelia cells [27–29], as found in this study, proliferate and extend inside the alveolar septa, and compress and diminish the alveoli. Our study showed that lepidic tumor cells were either hindered by the bronchioli and bronchus or got around them, or both, in the process of spreading along the alveolar septa, and correspondingly formed a well-defined margin and lobulation, an irregular shape, or spiculation. As the tumor cells aggregated, the growth pattern transitioned from lepidic to hilic and formed a partly solid or even solid nodule, which frequently squeezed and obliterated the alveoli and alveolar ducts, bronchioli, and bronchus. Therefore, as tumor size increased, few bronchiole and bronchus were found at the center of the tumor. Alternatively, as the solid component increased, fewer bronchiole and bronchus were found at the center periphery, and exterior border. In almost all partly solid tumors the bronchus was found at the exterior border, but the bronchus of totally solid tumors was less frequently found there.

### *The Relationship Between Early LAC and Bronchus in Mice*

As a result of LAC originating from the airway epithelium, the tumor causes the spatial relationship with the bronchus. The development of the tumor gradually leads to changes in bronchial morphology. Previous clinical studies [30] have indicated that CT demonstrated five types of tumor-bronchus relationships in 86% malignant and 76% benign nodules of less than 3 cm in diameter. The types are as follows: type I: bronchus was obstructed abruptly by the tumor; type II: bronchus penetrated into the tumor with tapered narrowing and interruption; type III: bronchial lumen shown within the tumor was patent and intact; types IV and V: bronchus ran around the periphery of the tumor with either intact lumen or displaced, compressed, and narrowed lumen. Malignant nodules had 59% of type I, 15% of type II, 15% of type III, 26% of type IV and 2% of type V. Types I, II, and IV were more common in malignant nodules than in benign nodules. The following studies obtained similar results [31–33]. In this study, similar manifestations were obtained by using micro-CT in mouse early LAC, and, thus, a similar classification was used. The first three types were the same as the clinical classification. Due to the small tumors and, consequently, little compression on border bronchus, type IV and type V could not be distinguished on micro-CT images. Thus, we merged type IV and type V into type IV; i.e., bronchus ran around the periphery of the tumor with an intact or compressed lumen.

Compared with that of previous studies, this study showed that the prevalence of each tumor-bronchus relationship was significantly different [29–32]. There were significantly fewer type I and more type IV in our micro-CT study. The mean diameter of tumors was only 0.56 mm, which was approximately equivalent to 11 mm of human lung tumors [16]. Small tumors lightly compressed border bronchioli, leading to less of type I and more of type IV tumor-bronchus relationship. As tumor size increased, the prevalence of type I increased and that of both type II and type III decreased. Furthermore, owing to the high resolution of 19 μm, micro-CT could display terminal bronchioli and alveolar ducts, and, thus, more subtle tumor-bronchus relationships could be observed. In previous clinical studies, most tumors were larger solid tumors that exerted great pressure on border bronchi and resulted in more type I and less type IV and type V tumor-bronchus relationships. In addition, the resolution of clinical CT was not high enough to show distal to seventh-order bronchi and led to less incidence of tumor-bronchus relationship.

This study had some limitations. First, in order to avoid motion artifact and indistinct image, micro-CT scan was performed in a euthanized and fixed mouse model. Second, because the trachea was ligated at the end of deep inspiration, the diameter of the bronchus might be slightly larger. Third, due to the lack of pathological criteria for mouse early LAC, we arbitrarily assumed early LAC according to the tumor size [16].

## Conclusion

Micro-CT can clearly demonstrate the imaging features of mouse early LAC and tumor-bronchus relationships. This technique provides both a new tool and a new perspective for the study of early LAC, affording new information for clinical CT diagnosis of early LAC.

## References


[1] Siegel R, Naishadham D, and Jemal A (2013). Cancer statistics, 2013. *CA Cancer J Clin*. http://dx.doi.org/10.3322/caac.21166.

[2] Ferlay J, Shin HR, Bray F, Forman D, Mathers C, and Parkin DM (2010). Estimates of worldwide burden of cancer in 2008: GLOBOCAN 2008. *Int J Cancer*. http://dx.doi.org/10.1002/ijc.25516.

[3] International Early Lung Cancer Action Program InvestigatorsHenschke CI, Yankelevitz DF, Libby DM, Pasmantier MW, Smith JP, and Miettinen OS (2006). International Early Lung Cancer Action Program Investigators: Survival of patients with stage I lung cancer detected on CT screening. *N Engl J Med*. http://dx.doi.org/10.1056/NEJMoa060476.

[4] National Lung Screening Trial Research TeamChurch TR, Black WC, Aberle DR, Berg CD, Clingan KL, Duan F, Fagerstrom RM, Gareen IF, and Gierada DS, et al (2013). Results of initial low-dose computed tomographic screening for lung cancer. *N Engl J Med*. http://dx.doi.org/10.1056/NEJMoa1209120.

[5] Henschke CI, McCauley DI, Yankelevitz DF, Naidich DP, McGuinness G, Miettinen OS, Libby DM, Pasmantier MW, Koizumi J, and Altorki NK, et al (1999). Early lung cancer action project: overall design and findings from baseline screening. *Lancet*. http://dx.doi.org/10.1016/S0140-6736(99)06093-6.

[6] Diederich S, Wormanns D, Semik M, Thomas M, Lenzen H, Roos N, and Heindel W (2002). Screening for early lung cancer with low-dose spiral CT: prevalence in 817 asymptomatic smokers. *Radiology*. http://dx.doi.org/10.1148/radiol.2223010490.

[7] National Lung Screening Trial Research TeamAberle DR, Adams AM, Berg CD, Black WC, Clapp JD, Fagerstrom RM, Gareen IF, Gatsonis C, and Marcus PM, et al (2011). Reduced lung-cancer mortalitywith low-dose computed tomographic screening. *N Engl J Med*. http://dx.doi.org/10.1056/NEJMoa1102873.

[8] Wahidi MM, Govert JA, Goudar RK, Gould MK, McCrory DC, and American College of Chest Physicians (2007). Evidence for the treatment of patients with pulmonary nodules: when is it lung cancer?: ACCP evidence-based clinical practice guidelines (2nd edition). *Chest*. http://dx.doi.org/10.1378/chest.07-1352.

[9] Tang AW, Moss HA, and Robertson RJ (2003). The solitary pulmonary nodule. *Eur J Radiol*. http://dx.doi.org/10.1016/S0720-048X(02)00297-8.

[10] Rubins JB and Rubins HB (1996). Temporal trends in the prevalence of malignancy in resected solitary pulmonary lesions. *Chest*. http://dx.doi.org/10.1378/chest.109.1.100.

[11] Devesa SS, Bray F, Vizcaino AP, and Parkin DM (2005). International lung cancer trends by histologic type: male:female differences diminishing and adenocarcinoma rates rising. *Int J Cancer*. http://dx.doi.org/10.1002/ijc.21183.

[12] Xing Y, Li Z, Jiang S, Xiang W, and Sun X (2014). Analysis of pre-invasive lung adenocarcinoma lesions on thin-section computerized tomography. *Clin Respir J*. http://dx.doi.org/10.1111/crj.12142.

[13] Sone S, Nakayama T, Honda T, Tsushima K, Li F, Haniuda M, Takahashi Y, Suzuki T, Yamanda T, and Kondo R, et al (2007). Long-term follow-up study of a population-based 1996–1998 mass screening programme for lung cancer using mobile low-dose spiral computed tomography. *Lung Cancer*. http://dx.doi.org/10.1016/j.lungcan.2007.06.022.

[14] Counter WB, Wang IQ, Farncombe TH, and Labiris NR (2013). Airway and pulmonary vascular measurements using contrast-enhanced micro-CT in rodents. *Am J Physiol Lung Cell Mol Physiol*. http://dx.doi.org/10.1152/ajplung.00281.2012.

[15] Hori Y, Takasuka N, Mutoh M, Kitahashi T, Kojima S, Imaida K, Suzuki M, Kohara K, Yamamoto S, and Moriyama N, et al (2008). Periodic analysis of urethane-induced pulmonary tumors in living A/J mice by respiration-gated X-ray microcomputed tomography. *Cancer Sci*. http://dx.doi.org/10.1111/j.1349-7006.2008.00889.x.

[16] Xiao SM, Zhang Y, and Qiang JW (2015). Establishment of a mouse model of early lung adenocarcinoma. *Acta Laboratorium Animalis Scientia Sinica*. http://dx.doi.org/10.3969/j.issn.1005-4847.2015.03.002.

[17] Rudyanto RD, Bastarrika G, de Biurrun G, Agorreta J, Montuenga LM, Ortiz-de-Solorzano C, and Muñoz-Barrutia A (2013). Individual nodule tracking in micro-CT images of a longitudinal lung cancer mouse model. *Med Image Anal*. http://dx.doi.org/10.1016/j.media.2013.07.002.

[18] Li M, Jirapatnakul A, Biancardi A, Riccio ML, Weiss RS, and Reeves AP (2013). Growth pattern analysis of murine lung neoplasms by advanced semi-automated quantification of micro-CT images. *PLoS One*. http://dx.doi.org/10.1371/journal.pone.0083806.

[19] Ashton JR, Clark DP, Moding EJ, Ghaghada K, Kirsch DG, West JL, and Badea CT (2014). Dual-energy micro-CT functional imaging of primary lung cancer in mice using gold and iodine nanoparticle contrast agents: a validation study. *PLoS One*. http://dx.doi.org/10.1371/journal.pone.0088129.

[20] Savai R, Wolf JC, Greschus S, Eul BG, Schermuly RT, Hänze J, Voswinckel R, Langheinrich AC, Grimminger F, and Traupe H, et al (2005). Analysis of tumor vessel supply in Lewis lung carcinoma in mice by fluorescent microsphere distribution and imaging with micro- and flat-panel computed tomography. *Am J Pathol*. http://dx.doi.org/10.1016/S0002-9440(10)61184-4.

[21] Savai R, Langheinrich AC, Schermuly RT, Pullamsetti SS, Dumitrascu R, Traupe H, Rau WS, Seeger W, Grimminger F, and Banat GA (2009). Evaluation of angiogenesis using micro-computed tomography in xenograft mouse model of lung cancer. *Neoplasia*. http://dx.doi.org/10.1593/neo.81036.

[22] Fushiki H, Kanoh-Azuma T, Katoh M, Kawabata K, Jiang J, Tsuchiya N, Satow A, Tamai Y, and Hayakawa Y (2009). Quantification of mouse pulmonary cancer models by microcomputed tomography imaging. *Cancer Sci*. http://dx.doi.org/10.1111/j.1349-7006.2009.01199.x.

[23] Paik SH, Kim WK, Park JS, Park CS, and Jin GY (2014). A quantitative study of airway changes on micro-CT in a mouse asthma model: comparison with histopathological findings. *Allergy Asthma Immunol Res*. http://dx.doi.org/10.4168/aair.2014.6.1.75.

[24] Xiao L, Sera T, Koshiyama K, and Wada S (2013). A semiautomatic segmentation algorithm for extracting the complete structure of acini from synchrotron micro-CT images. *Comput Math Methods Med*. http://dx.doi.org/10.1155/2013/575086.

[25] Chu ZG, Yang ZG, Shao H, Zhu ZY, Deng W, Tang SS, Chen J, and Li Y (2011). Small peripheral lung adenocarcinoma: CT and histopathologic characteristics and prognostic implications. *Cancer Imaging*. http://dx.doi.org/10.1102/1470-7330.2011.0033.

[26] Gardiner N, Jogai S, and Wallis A (2014). The revised lung adenocarcinoma classification-an imaging guide. *J Thorac Dis*. http://dx.doi.org/10.3978/-j.issn.2072-1439.2014.04.05.

[27] Mason RJ, Kalina M, Nielsen LD, Malkinson AM, and Shannon JM (2000). Surfactant protein C expression in urethane-induced murine pulmonary tumors. *Am J Pathol*. http://dx.doi.org/10.1016/S0002-9440(10)64717-7.

[28] Broers JL, Jensen SM, Travis WD, Pass H, Whitsett JA, Singh G, Katyal SL, Gazdar AF, Minna JD, and Linnoila RI (1992). Expression of surfactant associated protein-A and Clara cell 10 kilodalton mRNA in neoplastic and non-neoplastic human lung tissue as detected by in situ hybridization. Laboratory Investigation; 1992.

[29] Ten Have-Opbroek AA, Benfield JR, van Krieken JH, and Dijkman JH (1997). The alveolar type II cell is a pluripotential stem cell in the genesis of human adenocarcinomas and squamous cell carcinomas. *Histol Histopathol*.

[30] Qiang JW, Zhou KR, Lu G, Wang Q, Ye XG, Xu ST, and Tan LJ (2004). The relationship between solitary pulmonary nodules and bronchi: multi-slice CT-pathological correlation. *Clin Radiol*. http://dx.doi.org/10.1016/j.crad.2004.02.018.

[31] Liu XG, Wang Y, Liang MZ, Zhang H, Chen CF, Qin PX, Zhong GM, He YL, Hu XB, and Han MJ, et al (2008). The relationship between the peripheral lung cancer and the bronchi, pulmonary artery and vein: a muitislice helical CT observation. *Chin J Radiol*. http://dx.doi.org/10.3321/j.issn:1005-1201.2008.06.008.

[32] Cui Y, Ma DQ, and Liu WH (2009). Value of multiplanar reconstruction in MSCT in demonstrating the relationship between solitary pulmonary nodule and bronchus. *Clin Imaging*. http://dx.doi.org/10.1016/j.clinimag.2008.06.028.

[33] Sun PF, Xiao XS, Li HM, Yu H, and Liu SY (2008). Radiologic-pathologic study on bronchial changes in peripheral solitary pulmonary lesions. *Chin J Cancer*. http://dx.doi.org/10.3321/j.issn:1000-467X.2008.12.012.